AIP | Journal of Applied Physics

Anti-Stokes fluorescence imaging of microscale thermal fields in thin films

A. N. Kuzmin, A. Baev, A. V. Kachynski, T. S. Fisher, A. Shakouri et al.

Citation: J. Appl. Phys. **110**, 033512 (2011); doi: 10.1063/1.3606429
View online: http://dx.doi.org/10.1063/1.3606429
View Table of Contents: http://jap.aip.org/resource/1/JAPIAU/v110/i3
Published by the AIP Publishing LLC.

Anti-Stokes fluorescence imaging of microscale thermal fields in thin films

A. N. Kuzmin,[1] A. Baev,[1] A. V. Kachynski,[1] T. S. Fisher,[2] A. Shakouri,[3] and P. N. Prasad[1,a)]
[1]*The Institute for Lasers, Photonics and Biophotonics, State University of New York at Buffalo, Buffalo, New York 14260, USA*
[2]*Purdue University, Birck Nanotechnology Center, 1205 West State Street, West Lafayette, Indiana 47907-2057, USA*
[3]*University of California – Santa Cruz, Baskin Engineering 253A, 1156 High Street, Santa Cruz, California 95064-1077, USA*

(Received 22 December 2010; accepted 28 May 2011; published online 5 August 2011)

We demonstrate that the in-plane thin film heat transport can be accurately mapped via confocal anti-Stokes fluorescence imaging using fluorescent dye probes and nanoheaters. We employ 3D finite elements analysis to evaluate the thermal conductivity of a control sample and to assess the validity of a point heat source approximation. We have found that this approximation is adequate with use of a tightly focused laser beam, providing a robust means for determining the thermal conductivity of a sample under investigation. © *2011 American Institute of Physics*. [doi:10.1063/1.3606429]

I. INTRODUCTION

Thermoelectric materials constitute an important class of engineered materials with many civilian and military applications. Reliable and reproducible characterization of thermal transport in these materials is, therefore, of extreme importance for correct assessment of thermoelectric figure-of-merit. Traditional methods of measuring the thermal conductivity of bulk and film specimens include steady-state and transient techniques[1–7] based on monitoring the temperature difference between two spaced points in the studied material or over a time interval at a certain point, respectively. In this report, we demonstrate a novel non-contact technique based on anti-Stokes fluorescence confocal 3D imaging.[8,9] The anti-Stokes fluorescence technique is particularly suitable for micro- and sub-micro characterization of in-plane thermal transport in thin films and allows for both transient as well as steady-state regimes of characterization. The sub-microscale length regime, falling between sub-continuum and continuum transport physics, is of particular importance, as recent work has shown that material processing to create domain sizes in this regime offers substantial, though highly complex, improvements in thermoelectric performance.[10] It should be noted, that when applied to polymeric thin films, for average phonon Mean Free Path (MFP) in the range of 1 nm,[11] the optical resolution will not be able to capture the features of ballistic phonon transport, and therefore "sub-microscale" would simply mean the transport on the length-scale of the optical resolution of our setup (~500 nm).

An alternative method of micro-Raman spectroscopy confocal technique allows for the non-contact measurements of microscale thermal properties of materials. It does not require any staining of the sample and has been already successfully used for measurements of temperature gradients in semiconductor microchips.[12–14] However, in comparison to anti-Stokes fluorescence method, Raman signal intensity is usually several orders of magnitude lower, which requires longer image acquisition time (from several minutes to an hour) and, therefore, Raman technique can only be used in steady-state regime when equilibrium is well established. Raman temperature technique based on the measurements of wavelength shift of specific spectral peak requires sophisticated spectral equipment with extremely high spectral resolution of ~ 0.1 cm^{-1} (or higher) to reach temperature sensitivity $\sim 10\,^{\circ}$C. In addition, for Raman technique, temperature sensitivity does not depend on the excitation wavelength. In contrast, in case of thermal measurement by anti-Stokes fluorescence, the excitation wavelength can be tuned to an appropriate spectral region with respect to the fluorescence maximum of the probe to reach a temperature sensitivity of less than $1.0\,^{\circ}$C.

Conventional Stokes fluorescence is related to the optical excitation of fluorophore molecules from the lower densely populated vibrational levels of the ground electronic state and subsequent radiative decay from the excited to the ground state. Under stationary conditions and low excitation power, Stokes fluorescence intensity is weakly dependent on the temperature. In case of the anti-Stokes luminescence (ASL), the optical excitation is caused by absorption of photons with lower energy from thermally populated vibrational-rotational states of the ground electronic state. Since the population of the upper vibrational levels of the ground state is temperature dependent (based on Boltzmann distribution), the ASL intensity is extremely temperature dependent[15] (exponential dependence), as represented by the following equation: $I(T) \sim A \exp(-\Delta E/k_B T)$, where $I(T)$ is the ASL intensity of the dye solution at temperature T, A is a proportionality coefficient, k_B is the Boltzmann constant, and ΔE is the energy required to thermally populate a vibrational level. A detailed physical description and applications of the ASL for measuring local temperature variations can be found elsewhere.[15–18]

In our method, a probe dye and a heating agent - absorbing nanoparticles (NPs) with efficient non-radiative relaxation - are embedded into a film to be characterized.

a)Author to whom correspondence should be addressed. Electronic mail: pnprasad@buffalo.edu.

Absorption and emission wavelength bands of the dye (probe) and the heating agent (pump) are chosen to be spectrally separated from each other. Afterwards, the local heating generated by resonant pump absorption of nanoparticles creates a flow of heat through the film, both transverse and in-plane. In other words, we use the heating agent and absorbed energy of the pump to generate non-radiatively dissipated thermal field coupled to longitudinal acoustic phonons of the film matrix. At the same time, the probe beam (wavelength tuned to the red wing of the excitation spectrum) laterally scans the area nearby the heat source, which results in anti-Stokes fluorescence of the probe dye that is confocally detected. The rate and absolute value of thermal population, leading to anti-Stokes fluorescence, depend on the group velocity of phonons in the medium and the distance between the fluorophore and the source of phonons. Therefore, a mesoscopic thermal map can be created and certain important characteristics of local thermal transport in the medium can be extracted.

II. THEORY AND MODEL

The three-dimensional heat equation for a homogeneous medium reads

$$\frac{\partial u}{\partial t} - \alpha \nabla^2 u = q, \qquad \alpha = \frac{\kappa}{\rho c_p}, \tag{1}$$

where u is the temperature, α is the thermal diffusivity, κ is the thermal conductivity, ρ is the density, c_p is specific heat, and q is the rate of heat generated in the medium per unit volume divided by the product of mass density and specific heat. Numerical solution to this equation with initial and boundary conditions results in temporal and spatial distribution of the temperature of a sample, provided the macroscopic quantities κ, ρ, and c_p are known together with the parameters of the heat source. The inverse problem can be solved by fitting the solution of Eq. (1) to a temperature distribution created by a known volumetric heating field q. It has to be noted though that, according to Fourier's law taken in its integral form, the heat flux for a homogeneous isotropic medium through its surface is proportional to the negative temperature difference between the two points in one-dimensional case, where the proportionality coefficient is the thermal conductivity divided by the distance between the points. Moreover, if there is a steady supply of heat from a point source inside the volume, the solution of the Poisson's equation results in the width of the temperature distribution independent of the material parameters.[19] Therefore, if two samples that have absorbed, via embedded local heat sources, the same amount of energy have the same temperature difference over a length span, one can say, without loss of generality, that these two samples have the same thermal conductivity. This notion, in principle, makes numerical fitting unnecessary if two samples are measured and one of them has a known value of thermal conductivity. However, if the heat source is extended, numerical solution can give an additional insight into the problem. It should also be noted that, since nanoparticles absorption and/or non-radiative conversion can depend on the host medium, our assumption about the same amount of heat, produced in two different samples, is only true to a certain extent. We tried to circumvent this potential problem by using a thin layer of deposited NPs instead of NPs, dispersed in the bulk of the sample (see the description below).

To validate our premises, we used the COMSOL Multiphysics Finite Elements (FE) solver. It should be noted, that a semi-analytical solution could be used as well to solve the continuous heat equation assuming that the heat source is point-like. Here, we used FE to justify the validity of our point-like heat source assumption for adequate interpretation of our experimental results. In our numerical simulations FE analysis permits us to model the heat source by an extended cylinder-shaped solid heater with the geometry close to the experimental (focused Gaussian beam with lateral and axial focal waist size). Moreover, we have considered in our FE simulation the functional dependence of the amount of heat, generated inside the heater that followed the focused Gaussian beam intensity. Since the ratio of the temperature difference (between the peak value and the flat background) of the simulated temperature distributions turned out equal to the inverted ratio of the thermal conductivities of two polymeric samples probed in our study, we concluded that our heat source can be considered point-like. Furthermore, the numerical solution, obtained with FE analysis, resulted in the same ratio as obtained from solution of the Poisson's equation with a point source. In addition, FE model is more general and we could study more specific heat transfer phenomena, e.g. the effect of medium change near nanoparticles or anisotropic thermal properties (for very thin films), which will be the subject of our future studies. Details of the model are as follows. The computational domain spans 225 μm in the direction of laser beam propagation (z-axis) and 4 mm in both the x and y directions. Since the focused laser beam was used for heating a spot inside the sample, we modeled the heat source by a solid cylinder with the radius $w_0\sqrt{2}$ and height h, where $w_0 = 1$ micron is Gaussian beam waist and $h = 500$ nm is the thickness of nanoparticles (NPs) layer used as a heat source in our experimental design (see the experiment details below). The heat distribution within the source volume was defined to functionally follow the intensity distribution of the beam, since the excitation rate is proportional to the intensity and only absorbing NPs can generate heat due to non-radiative internal conversion. With the sample size much larger than the Gaussian spot size, this is an adequate approximation of a point heat source. We applied heat flux boundary conditions with convective cooling, $\mathbf{n} \cdot (\kappa \nabla T) = h(T_{amb} - T)$, to all external boundaries and found a thermal transient time of approximately 1 second for reaching steady state, in accord with experimental observations. The ambient temperature, T_{amb}, was set to 298 K. The numerical FEA model comprised 178 906 quadratic vector elements with 266 266 degrees of freedom.

III. EXPERIMENTAL SETUP AND SAMPLE PREPARATION

A simplified schematic for the imaging set-up is shown in Fig. 1. A 632.8 nm He-Ne laser (Meredith Instruments)

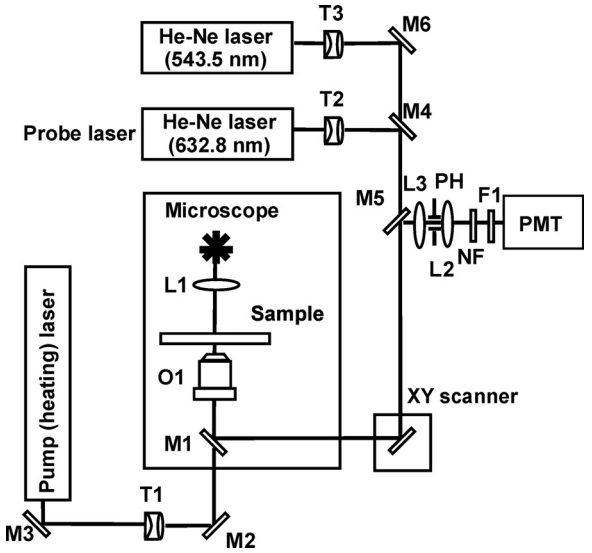

FIG. 1. Experimental setup. M1, M4, and M5 are dichroic mirrors; M2, M3, and M6 are mirrors; O1 is the objective lens; L1-L3 are lenses; T1-T3 are telescopes; PH is a pinhole, NF is a notch filter at 632 nm; F1 is a band filter for 535-650 nm.

with the output power of 20 mW and a 543.5 nm He-Ne laser (Melles Griot, 5mW) co-axially coupled to the same input microscope port were used as light sources to excite the anti-Stokes and the Stokes fluorescence, correspondingly, in a probe dye (Rhodamine 640) dispersed in a sample. A Nikon inverted microscope (Eclipse TE-2000-S) with the $60 \times \mathrm{NA} = 1.2$ Nikon objective lens was employed as a base for confocal microscopy to focus the pump and probe beams onto a sample. A picosecond optical parametric oscillator (Levante Emerald, APE) pumped by Nd:YVO_4 laser (picoTRAIN IC-10000/532-4000, HighQ Laser) was served as a pump source at 980 nm. The pump beam with the power of ~10 mW was coupled by a dichroic mirror into the same input microscope port, together with the 543.5 and 632.8 nm laser beams.

The anti-Stokes and the reference Stokes fluorescence signals were collected in the backward direction through the microscope objective lens and directed to the PMT by the spectrally separating dichroic mirror. The notch and the barrier filters extract the ant-Stokes fluorescence signal from the laser and other radiation backgrounds. The confocal microscopy mode was realized by the use of a pinhole of diameter ~70 μm in the focal plane of the focusing lens of the PMT detection system. A computer controlled XY galvano-scanner (GSI Lumonics), a Z stage (Piezosystem Jena), together with the detection system and a custom made software interface enabled for generation of optical image with the speed of 1 frame per second and with a resolution of 500×500 pixels. This experimental setup allowed in-plane (x, y) scanning the sample by the probe beam to obtain confocal imaging in the region near the stationary positioned IR pumped beam, within the area chosen by user through the software interface between 10×10 μm^2 and 290×290 μm^2. The probe beam waist diameter was estimated to be Ø0.8 μm, while the diameter of the pump beam waist was measured to be ~2 μm. Therefore, the in-plane resolution of obtained images was close to the wavelength of scanning laser beam ~0.6 μm. Due to the oblong shape of the probe beam in the Z-direction, the focal spot of the pump laser was aligned to be axial shifted to 2 $\mu m \pm 0.25$ backward to the scanning plane of the probe beam.

Solid film samples were prepared from the solution of either polymethyl methacrylate (PMMA) or polystyrene (PS) in chloroform. Rhodamine 640 was dissolved in chloroform with a concentration of about 0.15 M and then was added to polymer solution and stirred for ~2 hs. The next step of the sample preparation was the embedding $YbLiF_4$ nanoparticles (NPs), which played the role of nanoheaters, in the film. Two techniques were used for preparation of the polymer films with the NPs. A 0.1 wt% chloroform dispersion of ~10 nm diameter NPs was added to the polymer/dye solution and dispersed uniformly; then a composite film of thickness ~25 μm was formed by drying the mixture on a glass substrate (microscope coverslip) of $22 \times 22 \times 0.17$ mm^3 (PMMA-UDNP and PS-UDNP samples). Alternatively, a coverslip was coated by a thin layer of aggregated NPs (~ 500 nm) by evaporation of water from the aqua dispersion of the NPs encapsulated in a phospholipid micelle;[20] then the dye doped polymer solution was spin-coated on the top of the NP layer to form a layered structure (PMMA-LNP and PS-LNP samples). The second type of the sample, with a thin layer of deposited NPs, was used for experimental modeling of near-point heat source and ASL thermal imaging, having in mind that the pump beam focused onto the plane of NP layer will be absorbed by a tiny volume of NPs (~ Ø2 $\mu m \times 0.5$ μm) limited by the pump beam waist, which is at least 5 times smaller than in-plane size of generated thermal field (Fig. 2A). Correspondingly, this volume can be attributed to that of the source of local heating.

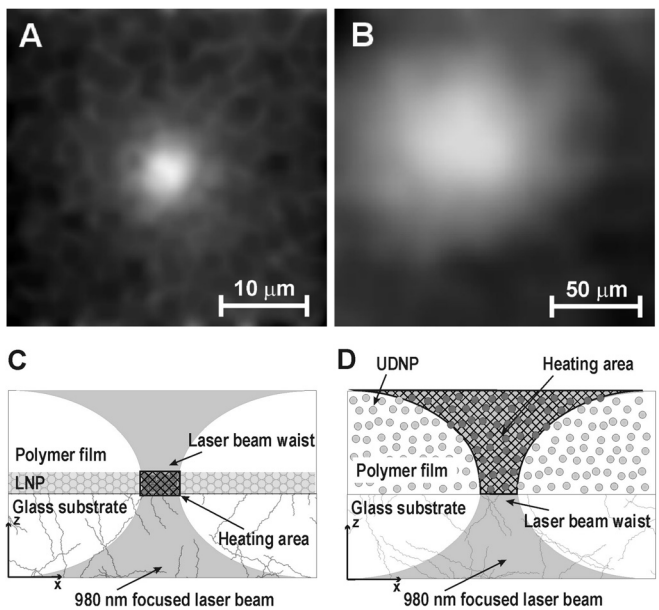

FIG. 2. Anti-Stokes images of heated area of polystyrene films with dispersed Rh640 as a probe dye and $YbLiF_3$ nanoheaters as a heating agent: (A) is an image of sample with layered structure; (B) is a picture obtained for film containing uniformly distributed NPs. The size of images: (A) 35×35 μm, (B) 200×200 μm. Dark background corresponds to the room temperature (~ 25 °C) ASL (C) and (D) are the layouts of LNP (C) and DUNP (D) samples and the corresponding schemes of laser induced heating.

IV. RESULTS AND DISCUSSION

Our experiments with a small size (mass) of the sample of the polymer films showed that a distinct temperature gradient appears after a lapse of several seconds following the turn-on of the heat source, when the transition processes are already over, but the average temperature of the sample has not increased significantly. Usually, this time interval lasts about 1-3 seconds and could be interpreted as a quasi steady-state.

Typical pictures of thermal images of the samples (described in Sec. II) acquired in the anti-Stokes fluorescence mode with local heating by a pump laser focused on the border of substrate and polymer film are shown in Fig. 2. To minimize the temperature image distortion caused by the local dye concentration inhomogeneity, the anti-Stokes images where normalized to the Stokes images, performed by 543.5 nm laser scanning. The thermal gradients generated by the same pump beam in the samples prepared by two different techniques (Fig. 2(A) presents the PS-LNP sample with thin NP layer; Fig. 2(B) - PS-UDNP sample with uniformly dispersed NP) demonstrate different slopes. A broad temperature distribution in the sample with uniformly dispersed $YbLiF_3$ nanoheaters (Fig. 2(B)) can be explained by non-localized absorption of the pump laser beam (Fig. 2(D)). In contrast to the spatially confined absorption in the thin layer of NPs, which corresponds to localized heating (Fig. 2(A,C)), uniformly dispersed NPs absorb the pump emission far away from the pump beam focus and the scanning plane, resulting in a cone like heating source. Most likely, this non-localized heating in the volume of the film produces a broad temperature distribution in the plane of confocal imaging (Fig. 2(B)).

Temperature distributions in the PMMA and PS films (prepared in the same technological conditions and pumped by the equal laser power) in the area near the heating source, obtained from 2D sections of the ASL in-plane images of layered samples, are shown in Fig. 3. Temperature calibration was performed by controlled uniform external heating of the samples.

The results of our modeling, based on numerical solution of Eq. (1), are presented in Fig. 4 and are superimposed with the experimental curves. For our fitting, we assumed that the mass density and specific heat of our material (polystyrene and PMMA) are known (1.05 g/cm^3 and 1.18 g/cm^3; 1.3 kJ/kg·K and 1.46 kJ/kg·K, correspondingly).[21,22]

We also assumed that the heating layer did not change thermal properties of the PS and PMMA samples.[23] The temperature distributions in (x,y) plane were recorded at 2 microns above the substrate, which corresponds to the focal plane of the scanning beam. For the thermal conductivities of polystyrene (0.08 W/m·K) and PMMA (0.15 W/m·K),[21,22] the ratio of temperature differences (differences are taken between 0 and 20 microns) agreed well with the experimental data obtained with the NPs layer as the heat source (see Figs. 3 and 4). At the same time, the amount of heat required to generate a temperature rise of 18 °C for the PS-LNP and 10 °C for the PMMA-LNP samples was found to be <1 mW from our fitting (heat density integrated over the volume of the heating body), which is in good agreement with transmission of both PS-LNP and PMMA-LNP samples at 980 nm ($\sim$1 mW). A comparison of the simulated temperature distribution for PS-LNP and PMMA-LNP samples with the experimental profile (Fig. 4) revealed an extra broadening of simulated distribution. The reason for this is the experimental uncertainty (± 0.25 μm) in the height of the scanning beam focal plane and the thickness of the NPs layer.

It is worthwhile to note that it would be beneficial to use a nonlinear mechanism of absorption (e.g., two-photon absorption) for excitation of our heat source. The advantage of nonlinear process is that, due to a higher power dependence on the excitation intensity, the excitation occurs in a spatially confined condition, which adequately corresponds to a sub-microscale heat transport process in approximation of a thermal point source. In principle, with our experimental technique, one can thermally excite different sites of a

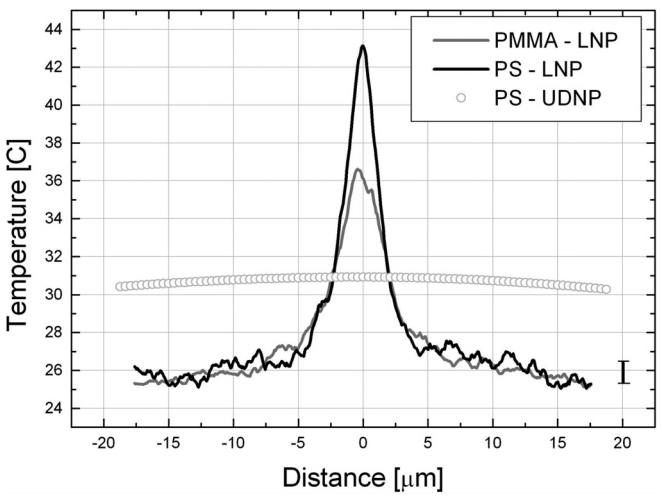

FIG. 3. Temperature distributions in the PMMA and PS films in the area near the heating source obtained by ASL imaging of the layered samples. LNP is the layered structure of NPs; UDNP is the uniformly dispersed NPs in the polymer film. Standard deviation for the experimental curves is shown as an error bar in left lower corner.

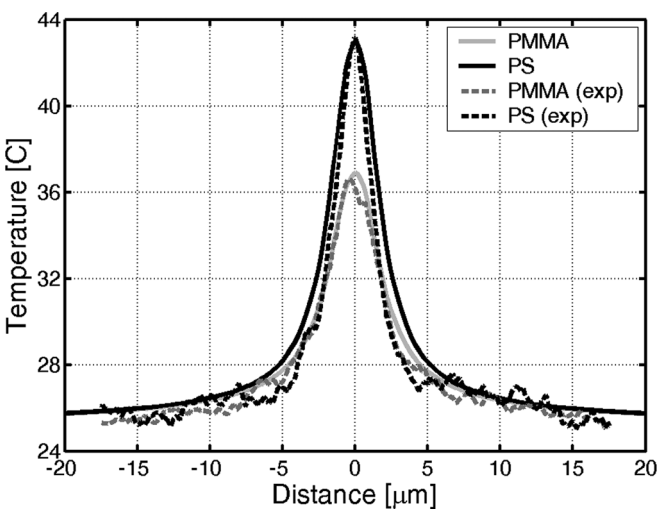

FIG. 4. Temperature distributions obtained with FE modeling vs experimental data.

sample and study the transient behavior of the temperature at a point separated by a few hundred nanometers from the heat source to monitor phonon transport in nanostructured materials, which is a subject of our future work. This is the key innovation of our work that could have an important impact for new developments in the area of high-efficient thermoelectric materials. Especially, this technology is very promising if different tag molecules are used to study temperature distribution in sub-hundred nanometers range, which is well below the diffraction limit of optical measurements. The concentration of nanoheaters in this case should be not more than one per micron squared.

IV. CONCLUSIONS

A novel non-contact technique for meso-scale characterization of phonon transport in thin film samples has been demonstrated. A point heat source has been realized experimentally and employed for a comparative study of thermal conductivities of two polymeric films. The ratio of thermal conductivities obtained in the experiment agreed well with that predicted by simulations. Potential application of anti-Stokes fluorescence technique to characterization of nano-scale thermal transport has been discussed. Having established the foundational for thermal applicability of this technique for the first time in the present work, we believe that its extension to the study of mesoscopic thermoelectric materials is readily achievable. The ability to create quantifiable and controlled local temperature gradients will enable the study of electrically functionalized thermoelectric films, for which thermal and thermoelectric property mapping can occur simultaneously.

ACKNOWLEDGMENTS

The authors are grateful to Guanying Chen for nanoparticles preparation and Tymish Ohulchanskyy for extensive discussions. This work was supported by a seed grant from the office of the Vice President for Research at the University at Buffalo.

[1]W. J. Parker, R. J. Jenkins, C. P. Butler, and G. L. Abbott, J. Appl. Phys. **32**, 1679 (1961).
[2]D. Chu, M. Touzelbaev, K. E. Goodson, S. Babin, and R. F. Pease, J. Vac. Sci. Technol. B **19**, 2874 (2001).
[3]K. E. Goodson, O. W. Kädling, M. Rösler, and R. Zachai, J. Appl. Phys. **77**, 1385 (1995).
[4]A. Rosencwaig and A. Gersho, J. Appl. Phys. **47**, 64 (1976).
[5]S. Govorkov, W. Ruderman, M. W. Horn, R. B. Goodman, and M. Rothschild, Rev. Sci. Instrum. **68**, 3828 (1997).
[6]N. O. Birge and S. R. Nagel, Rev. Sci. Instrum. **58**, 1464 (1987).
[7]D. G. Cahill and T. H. Allen, Appl. Phys. Lett. **65**, 309 (1994).
[8]A. V. Kachynski, A. N. Kuzmin, H. E. Pudavar, and P. N. Prasad, Appl. Phys. Lett. **87**, 023901 (2005).
[9]A. V. Kachynski, A. N. Kuzmin, H. E. Pudavar, and P. N. Prasad, U.S. Patent 7,413,341 (August 19, 2008).
[10]B. Poudel, Q. Hao, Y. Ma, Y. Lan, A. Minnich, B. Yu, X. Yan, D. Wang, A. Muto, D. Vashaee, X. Chen, J. Liu, M. S. Dresselhaus, G. Chen, and Z. Ren, Science **320**, 634 (2008).
[11]C. L. Choy, Polymer **18**, 984 (1977).
[12]T. Batten, A. Manoi, M. J. Uren, T. Martin, and M. Kuball, J. Appl. Phys. **107**, 074502 (2010).
[13]T. Beechem, S. Graham, S. P. Kearney, L. M. Phinney, and J. R. Serrano, Rev. Sci. Instrum. **78**, 061301 (2007).
[14]J. Christofferson, K. Maize, Y. Ezzahri, J. Shabani, X. Wang, and A. Shakouri. J. Electron. Packag. **130**, 041101 (2008).
[15]J. L. Clark, P. F. Miller, and G. Rumbles, J. Phys. Chem. A **102**, 4428 (1998).
[16]B. I. Stepanov and V. P. Gribkovskii, *Theory of Luminescence* (Iliffe Books Ltd., London, 1968).
[17]M. S. Chang, S. S. Elliott, T. K. Gustafson, C. Hu, and R. K. Jain, IEEE J. Quantum Electron. **8**, 527 (1972).
[18]J. L. Clark and G. Rumbles, Phys. Rev. Lett. **76**, 2037 (1996).
[19]H. S. Carslaw and J. C. Jaeger. *Conduction of Heat in Solids* (Oxford University Press, London, 1959).
[20]M. Nyk, A. Kuzmin, P. N. Prasad, W. Strek, and C. B. de Araújo, Opt. Mater. **31**, 800 (2009).
[21]*Polymer Data Handbook*, edited by J. E. Mark (Oxford University Press, New York, 2009).
[22]S. Rudtsch and U. Hammerschmidt, Int. J. Thermophys. **25**, 1475 (2004).
[23]D. J. Bergman and O. Levy, J. Appl. Phys. **70**, 6821 (1991).